SCIENTIFIC REPORTS

OPEN

Enhanced electrocaloric analysis and energy-storage performance of lanthanum modified lead titanate ceramics for potential solid-state refrigeration applications

Received: 16 August 2017
Accepted: 18 December 2017
Published online: 10 January 2018

Tian-Fu Zhang[1], Xian-Xiong Huang[1], Xin-Gui Tang[1], Yan-Ping Jiang[1], Qiu-Xiang Liu[1], Biao Lu[2] & Sheng-Guo Lu[2]

The unique properties and great variety of relaxer ferroelectrics make them highly attractive in energy-storage and solid-state refrigeration technologies. In this work, lanthanum modified lead titanate ceramics are prepared and studied. The giant electrocaloric effect in lanthanum modified lead titanate ceramics is revealed for the first time. Large refrigeration efficiency (27.4) and high adiabatic temperature change (1.67 K) are achieved by indirect analysis. Direct measurements of electrocaloric effect show that reversible adiabatic temperature change is also about 1.67 K, which exceeds many electrocaloric effect values in current direct measured electrocaloric studies. Both theoretical calculated and direct measured electrocaloric effects are in good agreements in high temperatures. Temperature and electric field related energy storage properties are also analyzed, maximum energy-storage density and energy-storage efficiency are about 0.31 J/cm^3 and 91.2%, respectively.

Since the discovery of ferroelectrics, ferroelectric materials have been exploited in many applications, such as: piezoelectric energy harvesting, optical electronic devices, and *etc*[1–3]. The unique properties and great variety of relaxer ferroelectrics also make them highly attractive for future solid-state refrigeration technologies. During the past decades, intensive research efforts have been conducted to develop solid-state cooling technologies[3,4]. The adiabatic temperature change (ΔT) and isothermal entropy change (ΔS) of polar materials are figure of merits of electrocaloric effect (*ECE*) during application and removal of electric field, which is environment friendly. *ECE* provides a highly efficient approach to achieve solid-state cooling instead of the existing vapour-compression refrigeration[5–9]. Recently, ferroelectrics for future solid-state refrigeration technologies become very hot[10–18]. In order to gain higher ΔT, many scholars pay attentions to thin films due to their large breakdown field[19–21]. It is a well-known fact that thin films have advantages in small solid state cooling devices, but bulk materials play an important role on larger scale devices, such as: refrigeration[22,23]. As a result, *ECE* of bulk materials are also desired, we should pay more attentions to *ECE* of bulk materials. Bulk materials including multilayer capacitors, ceramics and single crystals have been reported a lot, such as: $0.9Pb(Mg_{1/3}Nb_{2/3})O_3$–$0.1PbTiO_3$ multilayer capacitors[16], 0.9PMN-0.1PT single crystal[14], $Ba_{1-x}Sr_xTiO_3$ ceramics[12]. Compared to multilayer capacitors and single crystals, ceramics have the advantages of low-cost and easier fabrications.

In recent years, lead titanate (PT) based ceramics become one of the most studied and used ferroelectric materials in both scientific and industrial communities due to its high Curie temperature (T_c) and low dielectric constant[24,25], which make PT based ceramic to be a valuable research object[26–30]. In this work, lanthanum modified lead titanate ceramics $(Pb_{1-x}La_x)Ti_{1-x/4}O_3$ (PLT100x, $x = 0.20$, 0.24, 0.28, and 0.32, abbreviated as PLT20, PLT24, PLT28 and PLT32 respectively) ceramics are prepared and studied. Energy-storage and *ECE* of PLT ceramics are

[1]School of Physics & Optoelectric Engineering, Guangdong University of Technology, Guangzhou Higher Education Mega Center, Guangzhou, 510006, People's Republic of China. [2]School of Materials & Energy, Guangdong Province Key Lab Function Soft Matter, Guangdong University of Technology, Guangzhou Higher Education Mega Center, Guangzhou, 510006, People's Republic of China. Correspondence and requests for materials should be addressed to X.-G.T. (email: xgtang@gdut.edu.cn)

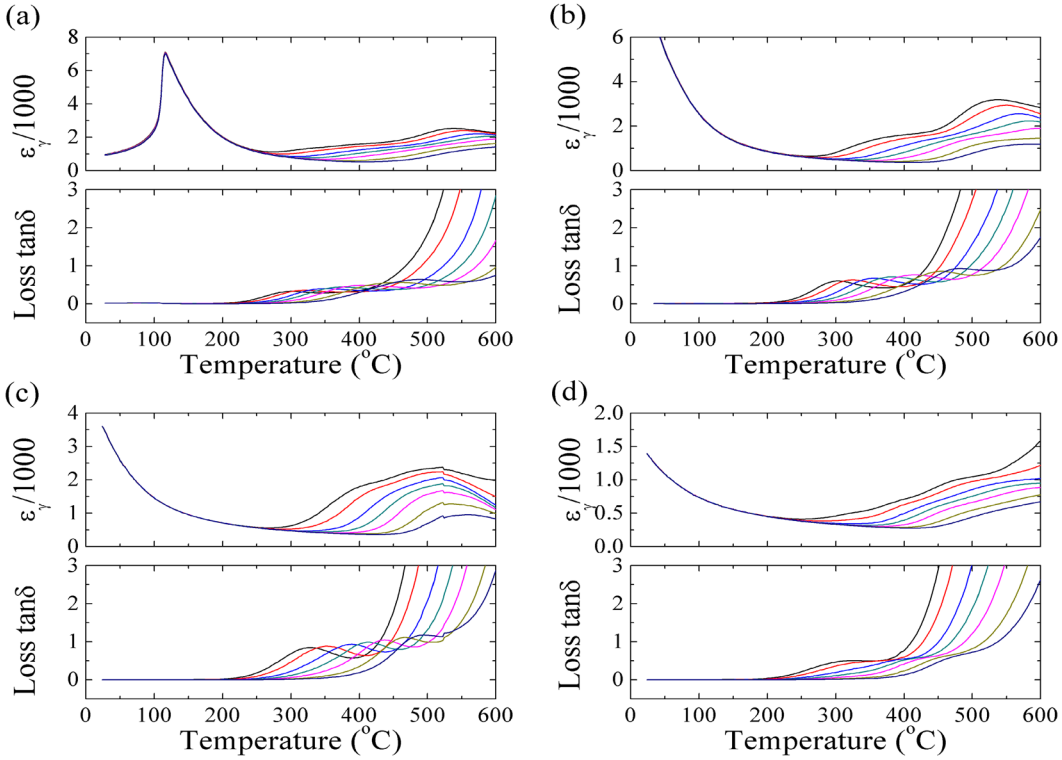

Figure 1. Dielectric permittivity ε_γ and dielectric loss *tanδ* as a function of temperatures for (**a**) PLT20, (**b**) PLT24, (**c**) PLT28 and (**d**) PLT32 ceramics with various measured frequencies (1, 2, 5, 10, 20, 50 and 100 kHz).

revealed for the first time. In this work, frequencies and temperatures dependent dielectric permittivity ε_γ and loss *tanδ* are also investigated to study the relaxer phase transitions and defects related relaxations. Ferroelectric based energy-storage properties are also analyzed. Energy-storage density in this work researches about 0.31 J/cm^3, high energy-storage efficiency (91.18%) is also obtained. Large *ECE* in PLT ceramics is achieved for the first time, maximum value of ΔT is about 1.67 K, and giant refrigeration efficiency is up to 27.4. Additional direct measured electrocaloric effects are analyzed, giant temperature change (1.67 K) is achieved, which indicates that PLT ceramics may be used in future solid-state refrigeration applications.

Experimental

PLT ceramics were synthesized by a conventional high temperature solid-state fabrication method. Reagent-grade Pb_3O_4, La_2O_3 and TiO_2 powders were weighted according to their stoichiometric composition. Then powders were first mixed and calcined at 850 °C for 5 h. The calcined powders were then mixed with alcohol milling for 24 h and dried. After that, powders were mixed thoroughly with a polyvinyl alcohol (PVA) binder solution and pressed into discs of 10 mm in diameter and 1 mm in thickness uniaxially. These discs were sintered at 1300 °C for 2 h in air. Silver paste was applied on both sides of discs and fired at 650 °C as electrodes for electrical properties measurements. High temperature dielectric behaviours were measured by Agilent E4980A (measure conditions: 0.5–1000 kHz, 25–600 °C). Low temperature permittivity ε_γ and dielectric loss *tanδ* of PLT samples were measured using an HP4194A LCR (measured conditions: 0.1–100 kHz, −193–165 °C). Complex impedance plots were conducted by Agilent E4980A (0.02–2000 kHz). Ferroelectric hysteresis loops were obtained by a computer-controlled virtual-ground circuit with Precision Premier II Ferroelectric Tester (Radiant Technologies, Inc., Albuquerque, New Mexico, USA). The direct measurements of *ECE* were conducted by a customized system: for the direct measurement, *ECE* change of temperature was monitored by a small thermistor attached to the upper gold electrode of ceramic. In order to reduce the heat exchange with environment, a thermistor and an electric field controlled by a computer were employed to detect the temperature change caused by *ECE* as the application or withdrawing of an electric field. Also, a high voltage generator controlled by an arbitrary signal generator is used to generator the electric field step signal, which is then applied to the sample. The voltage should be maintained for a few seconds to get into thermal equilibrium with the surrounding. Then the voltage was released immediately. The typical thermal response times along the sample thickness direction is a few milliseconds. Within such a short period, a very fast equilibration of the temperature throughout the whole sample, including the electrodes, attached thermistor and wires, took place, but then the equilibrated sample exchanges the heat on a much longer time scale to the surrounding bath.

Results and Discussion

Temperatures dependent dielectric permittivity ε_γ and loss *tanδ* for PLT samples are shown in Fig. 1 (Room temperature to 600 °C) and Fig. 2 (Lower temperatures: −193–165 °C). From Fig. 2, Temperature dependent ε_γ

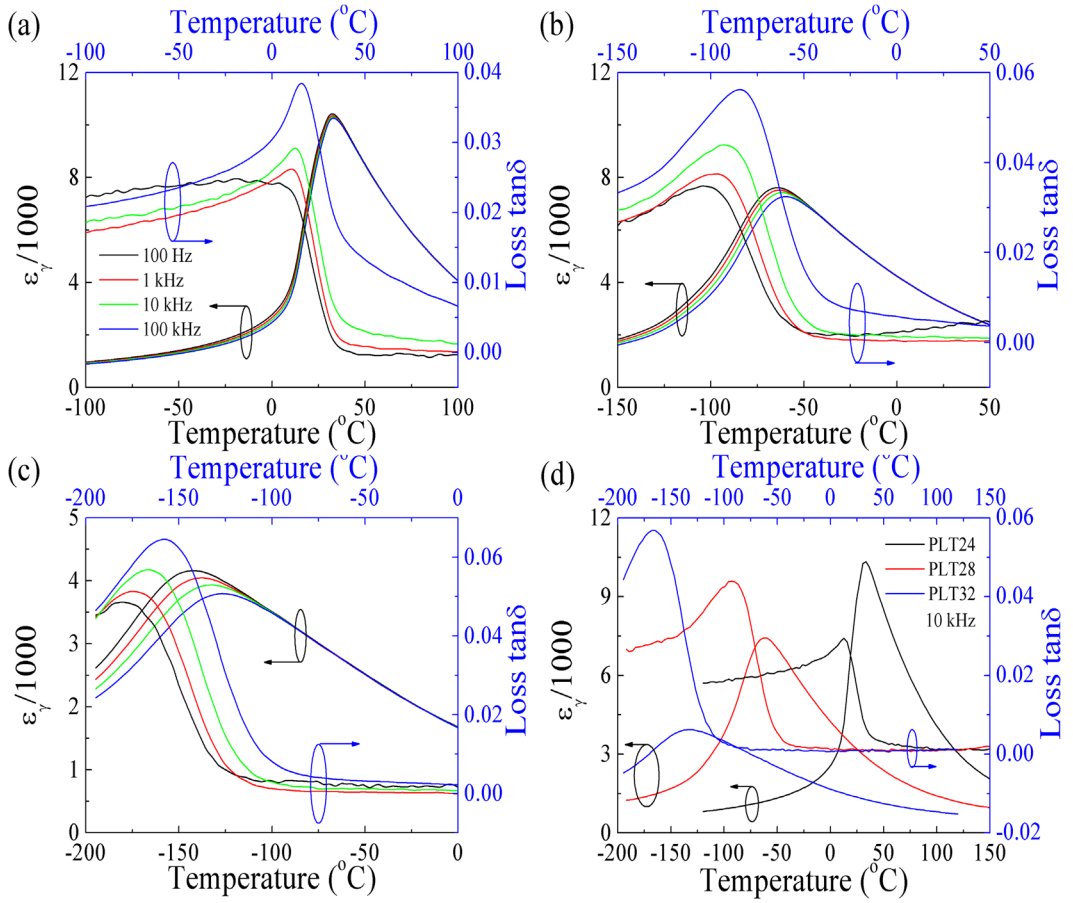

Figure 2. Dielectric permittivity ε_γ and dielectric loss *tan*δ as a function of temperatures for (**a**) PLT24, (**b**) PLT28 and (**c**) PLT32 ceramics, (**d**) three samples at 10 kHz.

depicts typical relaxer behaviours with a strong dispersion of ε_γ peaks, especially for PLT28 and PLT32 ceramics, T_m (temperature of maximum ε_γ) shift to higher temperatures and maximum ε_γ decrease with increasing frequencies. On the other hand, loss *tanδ* also exhibits broad peaks clearly, with increasing frequencies, maximum loss *tanδ* increase as well. Similar results were also reported[31,32]. This phenomenon signifies relaxer behaviours[33].

Generally speaking, the maximum value of ε_γ, at the Curie point T_c of an ideal ferroelectric crystal can be described by the Curie-Weiss law[34]:

$$1/\varepsilon_\gamma = (T - T_o)/C, \ (T > T_C) \tag{1}$$

where C and T_o are Curie-Weiss constant and Curie-Weiss temperature, respectively. For a first-order phase transition, T_C is greater than T_o, whereas for second-order phase transitions, T_C equals T_o[34]. In this work, ε_γ of PLT ceramics are analyzed by the Curie-Weiss law, plots of temperatures versus inverse ε_γ (at 10 kHz) are shown in Fig. 3. T_m and T_o are 385.15 K and 400.00 K, 306.49 and 335.68 K, 207.39 K and 265.75 K, 132.09 and 200.00 K respectively for PLT20, PLT24, PLT28, and PLT32 ceramics. Clearly, both T_m and T_o decrease sharply with increasing La concentrations.

It is well known that dielectric behaviours of relaxer ferroelectrics exhibit to deviate from typical Curie-Weiss behaviour, it can be described by a modified Curie-Weiss relationship[35]:

$$1/\varepsilon_\gamma - 1/\varepsilon_m = (T - T_m)^\gamma/C_1, \ (1 \le \gamma \le 2) \tag{2}$$

where C_1 and γ are assumed to be constant, and ε_m is the maximum permittivity. Parameter γ shows clear information on the character of phase transitions[36–38]. Figure 3 shows the plots of $\ln(1/\varepsilon_\gamma - 1/\varepsilon_m)$ versus $\ln(T - T_m)$ with (at 10 kHz). After fitting the experimental data to the modified Curie-Weiss relationship, we obtain the value of parameter $\gamma = 1.39$, 1.47, 1.66, 1.75, respectively for PLT20, PLT24, PLT28 and PLT32 ceramics. Fitting values of γ also support the evidence of relaxer nature.

From Fig. 1, it is found that abnormal dielectric peaks in permittivity and loss are observed (higher temperature region), similar behaviours are also reported in other perovskites (10–10^7 Hz, 400–800 °C), which are called dielectric relaxation[38–41]. In order to give a clear knowledge of high temperature dielectric relaxations, impedance technology is selected as an efficient technique, which has been intensive used in electrical properties of electro-ceramic materials[42]. The variation of normalized imaginary parts of impedance (Z''/Z''_{max}) are shown in

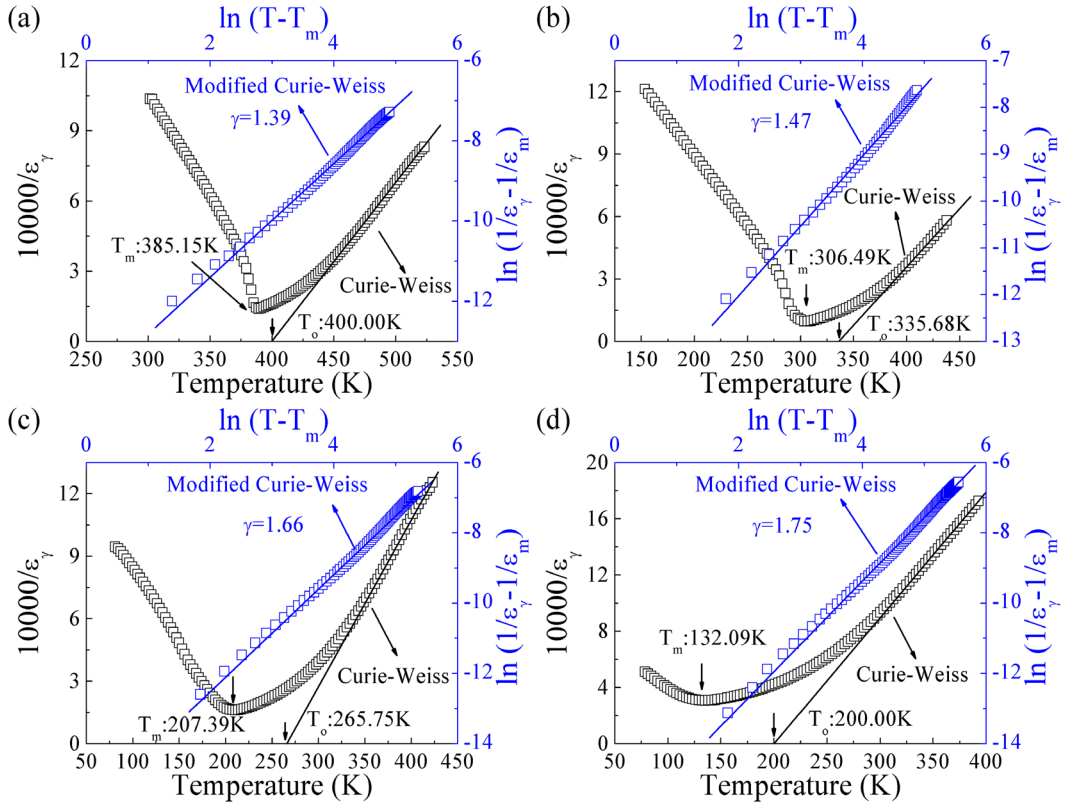

Figure 3. The inverse of dielectric permittivity ($10000/\varepsilon_\gamma$) as a function of temperature at 10 kHz (The black solid lines are used to fit the Curie-Weiss law), and the plot of $\ln(1/\varepsilon_\gamma - 1/\varepsilon_m)$ as a function of $\ln(T - T_m)$ for PLT ceramics measured at 10 kHz (The blue solid lines are a fit of modified Curie-Weiss relationship) respectively for (**a**) PLT20, (**b**) PLT24, (**c**) PLT28 and (**d**) PLT32 ceramics.

Fig. 4. Clearly, values of Z''/Z''_{max} become close gradually in higher frequencies. For PLT24 and PLT28 ceramics, Z''/Z''_{max} can be fitted into 2 separate parts. For a thermally activated relaxation process, relaxation frequency usually follows the Arrhenius law:

$$\omega = \omega_o \cdot exp(-E_a/k_\beta T) \tag{3}$$

where T, ω_o, E_a, k_β are the absolute temperature, characteristic frequency, activation energy and Boltzmann constant, respectively. Relaxation parameter E_a is determined by plotting $ln(\omega)$ as a function of the inverse of temperature ($1000/T$) using Arrhenius law (shown in Fig. 5). Two independent activation energies are obtain for PLT24 and PLT28 ceramics, grains (high frequency) and grain boundaries (low frequency) related activation energies are 1.60 eV and 1.82 eV, 1.15 eV and 1.66 eV respectively. Values of grain boundaries related activation energy are higher than those of grains, this indicate that grain boundaries exhibit higher resistance than grains[43]. For PLT20 and PLT32 ceramic, activation energies are about 1.73 and 1.75 eV respectively. For all compositions, values of activation energies are very close to OVs related high temperature dielectric relaxations in perovskite systems, such as: $SrTiO_3$[44], $(PbLa)(Zr_{0.9}Ti_{0.1})O_3$[45], and (Pb,Cd,La)$TiO_3$ ceramics[42].

Figure 6a shows polarization-electric field (*P-E*) hysteresis loops of PLT ceramics under various electric fields (30–60 kV/cm, ~300 K, 20 Hz). Typical ferroelectric hysteresis loops are observed for PLT20 and PLT24 ceramics, which manifests the ferroelectric phase at room temperatures. For PLT28 and PLT32 ceramics, slim hysteresis loops are achieved indicating the relaxer ferroelectric nature. At room temperature, remnant polarization, and coercive field decrease sharply with increasing La concentrations as shown in Fig. 6b.

As a well-known fact, *P-E* hysteresis loops also reflect energy-storage capacities of dielectric materials. According to the definition of energy-storage density by *P-E* hysteresis loops, energy-storage density, J_{reco}, is defined as[46–49]:

$$J_{reco} = \int EdP \tag{4}$$

Based on the above formula, J_{reco} can be obtained by numerical integration of the area between polarization axis and curves of *P-E* loops easily. In this work, energy-storage density J_{reco} (blue area, shown in Fig. 7a) calculated from *P-E* loops are about 0.19, 0.23, 0.31 and 0.18 J/cm^3 respectively for PLT20, PLT24, PLT28 and PLT32 ceramic (at 60 kV/cm). From the aspect of practical application, high energy-storage efficiency (η) and low energy-loss density (J_{loss}) are also significant. Similar to energy-storage density (J_{reco}), energy-loss density J_{loss} (the

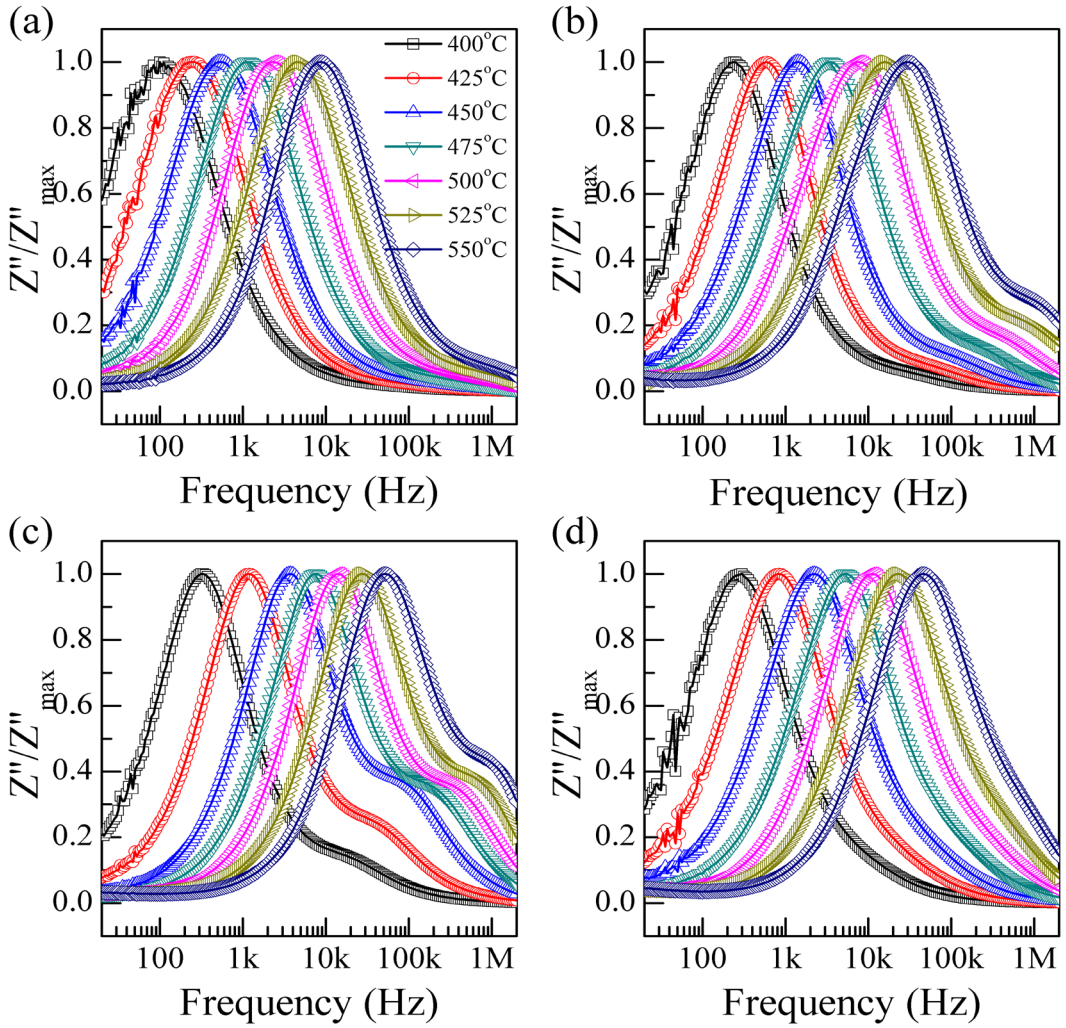

Figure 4. Normalized imaginary parts Z''/Z''_{max} of impedance as a function of frequencies for (**a**) PLT20, (**b**) PLT24, (**c**) PLT28 and (**d**) PLT32 ceramics.

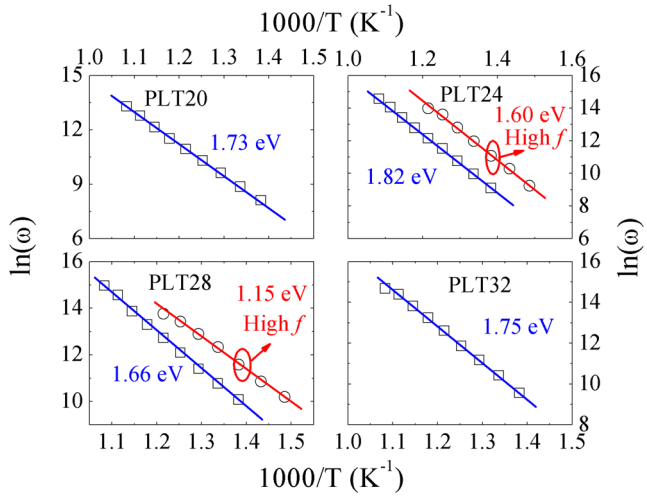

Figure 5. lnω versus 1000/T curves for PLT ceramics, straight lines are used to fit the Arrhenius law.

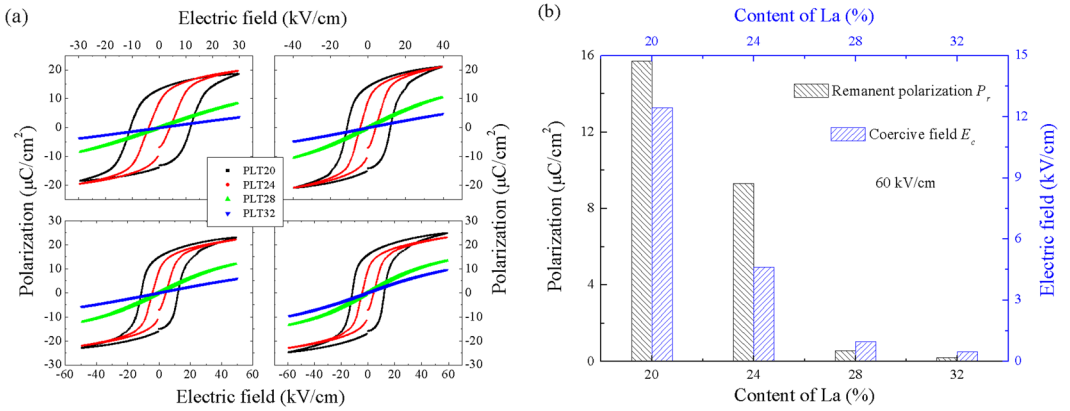

Figure 6. (**a**) *P-E* loops of PLT ceramics measured under various electric fields for PLT20 (black line), PLT24 (red line), PLT28 (blue line), PLT32 (magenta line). (**b**) Comparison of remanent polarization and coercive field of all samples.

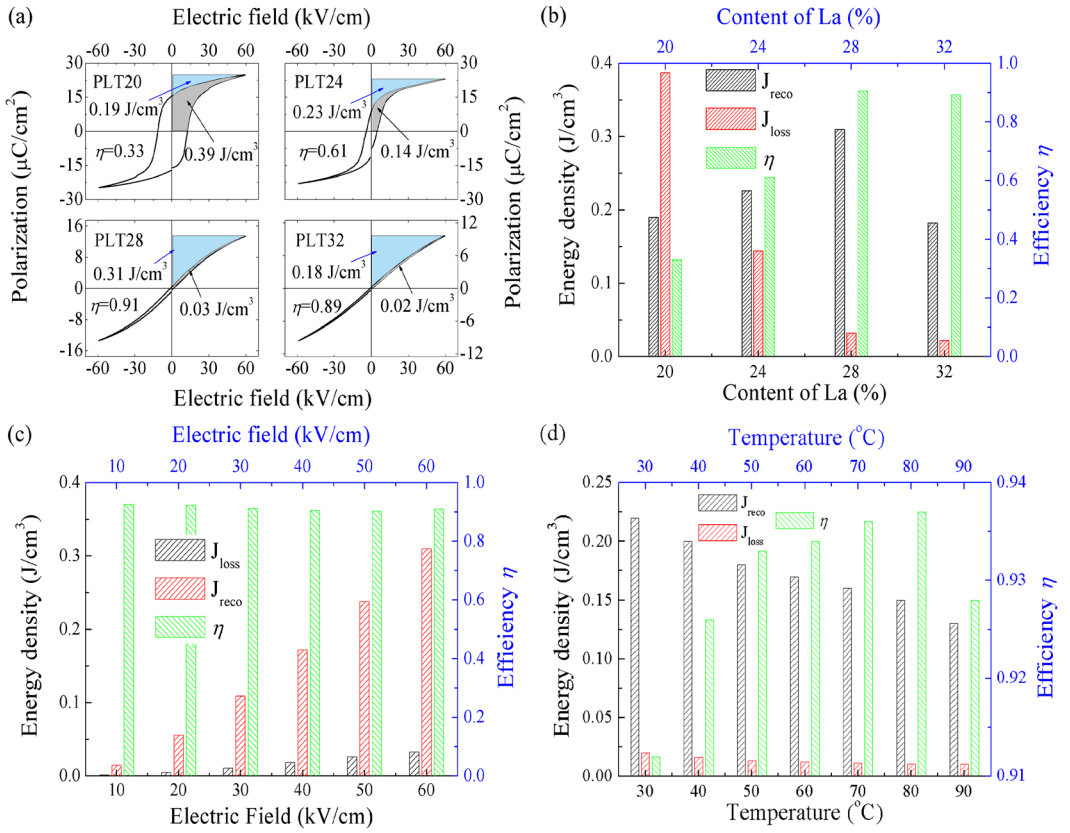

Figure 7. (**a**) Energy storage density calculated from *P-E* hysteresis loops of PLT ceramics, the blue area and the gray area showed the energy-storage density and energy-loss density, respectively. (**b**) Energy-storage properties with as a function of La concentrations. (**c**) Electric fields and (**d**) temperatures influenced energy-storage properties of PLT28 ceramic.

gray area, shown in Fig. 7a) can also be calculated from *P-E* loops. Results revealed that J_{loss} was about 0.39, 0.14, 0.03 and 0.02 J/cm^3 for PLT20, PLT24, PLT28 and PLT32 ceramic. Energy-storage efficiency η is defined as[50–53]:

$$\eta = J_{reco}/(J_{reco} + J_{loss}) \quad (5)$$

Accordingly, room temperature energy-storage efficiency of PLT ceramics according to the above formula are about 33%, 61%, 91%, and 89% respectively for PLT20, PLT24, PLT28 and PLT32 ceramic. Figure 7b shows the influence of La concentrations on the energy-storage properties. Clearly, PLT28 shows better energy-storage properties.

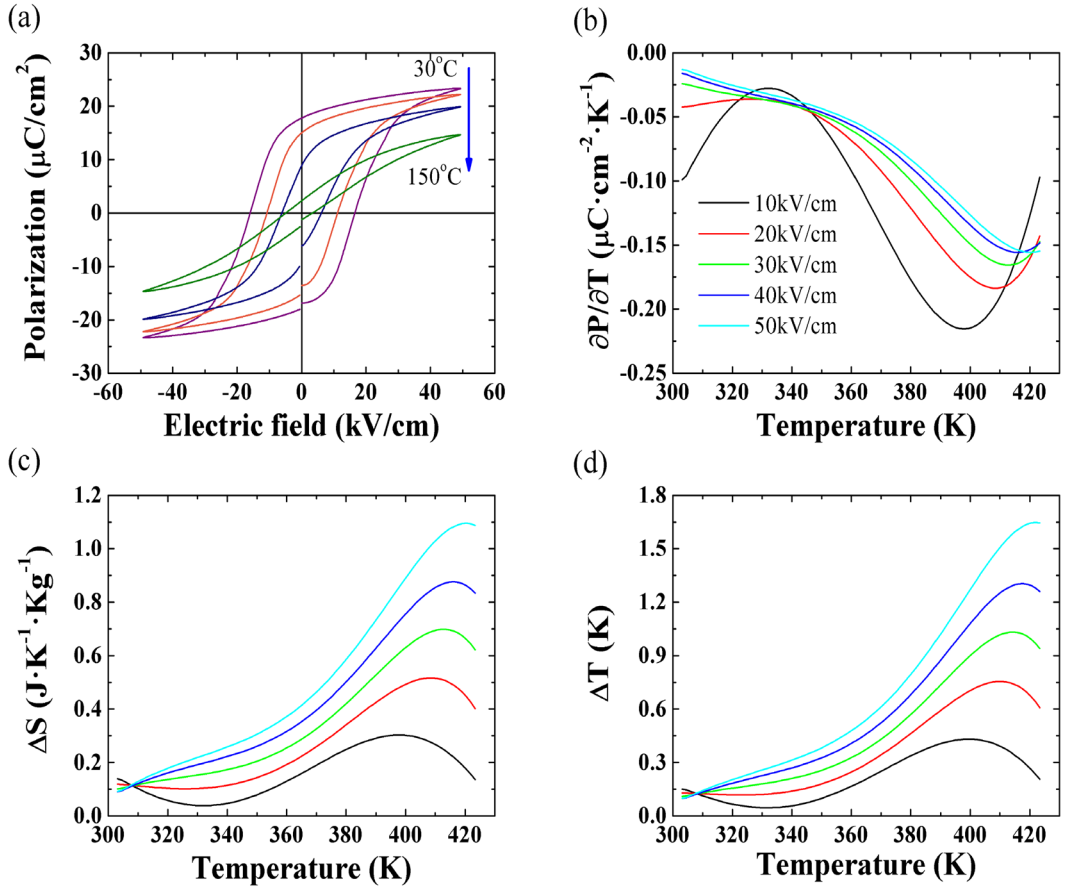

Figure 8. (**a**) Temperature dependent ferroelectric hysteresis loops. (**b**) $\partial P/\partial T$ curves of PLT20 samples. (**c**) The isothermal entropy change ΔS and (**d**) reversible adiabatic temperature change ΔT obtained from *P-E* data.

Due to the higher energy-storage density and efficiency of PLT28, PLT28 ceramics are chosen to study the influence of measured temperatures and electric fields on energy-storage properties (shown in Fig. 7c,d). Clearly, both J_{reco} and J_{loss} increase sharply with increasing electric fields, because larger electric field can induce higher polarization, and higher polarization will increase energy-storage density inevitably, but η keeps stable under various electric fields (>90%) (See Fig. 7c). With increasing temperatures, both J_{reco} and J_{loss} decrease sharply due to the decreasing of polarizations, but η exhibits the maximum value at 80 °C.

In this work, our results show lower values of J_{reco} than $(Pb_{0.91}La_{0.09})(Zr_{0.65}Ti_{0.35})O_3$ relaxer ferroelectric thin films[54], $PbZrO_3$ antiferroelectric thin films[55], HfO_2-ZrO_2 solid solution thin films[56], and $HfZrO_2$ films[53], those works report very good results, the energy storage densities are rather large. Compared with bulk materials, our results of J_{reco} are higher than $BaTiO_3$-$SrTiO_3$ composites[57], $BaSrTiO_3$ ceramics[58], $Sr_{0.5}Ba_{0.5}Nb_2O_6$ glass-ceramics[59], and *etc*. From aspects of applications, the priority among priorities for energy-storage devices are to gain a slim hysteresis loop (large saturated polarization, weak coercive field and small remanent polarization) or double hysteresis loops, this is the research direction to which we should pay more attentions[47,52].

In order to calculate *ECE* of ceramics, ferroelectric properties of PLT20 (50 kV/cm, 30–150 °C) are showed in Fig. 8a. Values of saturated polarization decrease with increasing temperatures. According to the principle of *ECE*, when electric field increases from E_1 to E_2, the isothermal entropy change ΔS of an *ECE* material should be:

$$\Delta S = S(E_1, T) - S(E_2, T) \tag{6}$$

Therefore, initial conditions of *ECE* materials at E_1 (in most cases, $E_1 = 0$) will affect *ECE* directly. Assuming the Maxwell relation:

$$(\partial P/\partial T)_E = (\partial S/\partial E)_T \tag{7}$$

The corresponding isothermal entropy change ΔS and the reversible adiabatic temperature change ΔT are calculated by following relations[60,61]:

$$\Delta S = -1/\rho \cdot \int (\partial P/\partial T)_E dE \tag{8}$$

Material	E(kV/cm)	T(K)	ΔT_{max}(K)	ζ_{max}(K·cm·kV^{-1})	Method	Material
PLT(This work)	50	420	1.67	0.033	Indirect	Ceramic
$0.75Bi_{1/2}Na_{1/2}TiO_3$-$0.25SrTiO_3$[64]	40	375	≈0.4	0.010	Indirect	Ceramic
$0.92Na_{0.5}Bi_{0.5}TiO_3$-$0.8BaTiO_3$[65]	50	413	−0.33	−0.007	Indirect	Ceramic
$BaHfTiO_3$[66]	50	338	1.35	0.027	Indirect	Ceramic
$Ba_{0.65}Sr_{0.35}TiO_3$[67]	90	303	2.10	0.023	Indirect	Ceramic
$0.9Pb(Mg_{1/3}Nb_{2/3})O_3$-$0.1PbTiO_3$[68]	57	380	≈1.25	≈0.0220	Indirect	Ceramic
$Pb_{0.85}La_{0.1}(Zr_{0.65}Ti_{0.35})O_3$[69]	200	—	3.1	0.0155	Indirect	Ceramic

Table 1. Comparison of *ECE* reported in this work with other bulk materials. T: Measured temperature.

$$\Delta T = -T/C\rho \cdot \int (\partial P/\partial T)_E dE \tag{9}$$

where ρ, C, E_1 and E_2 are mass density, mass heat capacity, initial and final applied electric fields, respectively. Values of $(\partial P/\partial T)_E$ (shown in Fig. 8b)can be obtained from the numerical differentiation of polarization-temperature data, which are extracted from upper branches of P-E loops ($E > 0$) measured at various temperatures.

ΔS and ΔT calculated at different electric fields are presented in Fig. 8c,d. Both ΔS and ΔT decrease firstly and then increase with increasing temperatures sharply (<30 kV/cm). On the other hand, ΔS and ΔT increase continuously with increasing temperatures especially for higher fields (>30 kV/cm). Temperatures of maximum ΔT (T_{ECmax}) shift toward the higher temperatures with increasing electric fields. Although the ΔT value in this study is lower than $PbZr_{0.95}Ti_{0.05}O_3$ film[19], PMN-PT films[62]. But for bulk materials, our results show higher values of ΔT than $Ba(Zr_{0.2}Ti_{0.8})O_3$-$(Ba_{0.7}Ca_{0.3})TiO_3$ ceramics[13], and $Sr_{0.75}Ba_{0.25}Nb_2O_6$ materials[63]. More comparison results[64–69] are shown in Table 1.

In order to give a comparison criterion for electrocaloric refrigeration, refrigeration efficiency is given:

$$COP = |Q|/|W| = |\Delta S \times T|/W \tag{10}$$

where Q and W are isothermal heat and corresponding electrical work per unit volume, and W is equal to $\int EdP$[70,71]. Our result reveals that value of COP for is about 27.4, which is much higher than previous reports of $Pb_{0.97}La_{0.02}(Zr_{0.75}Sn_{0.18}Ti_{0.07})O_3$ thick film ($COP = 18$)[70], $PbZr_{0.95}Ti_{0.05}O_3$ film[19], P(VDF-TrFE) film[72], and PMN-PT ($COP = 5.6$) films[62]. Large values of COP suggest the high cooling efficiency, which implies PLT20 ceramics have potential applications in future solid-state refrigeration technologies.

In order to evaluate the quantitative effect of electric field ΔE on *ECE*, electrocaloric coefficient is given:

$$\zeta_{max} = \Delta T_{max}/\Delta E_{max} \tag{11}$$

where ΔT_{max} is the maximum temperature change and ΔE_{max} is the corresponding electric field change[70]. Clearly, maximum ζ_{max} achieved in this work is 0.033 K·cm·kV^{-1}, which is higher than $(Pb_{0.97}La_{0.02})(Zr_{0.67}Sn_{0.38}Ti_{0.05})O_3$ thick films (0.030 K·cm·kV^{-1})[73], $BaZr_{0.2}Ti_{0.8}O_3$ ceramic[74], and $0.94Bi_{0.5}Na_{0.5}TiO_3$-$0.06KNbO_3$ ceramic[75], $0.7Pb(Mg_{1/3}Nb_{2/3})O_3$-$0.3PbTiO_3$ (0.03 K·cm·kV^{-1})[15], $0.9Pb(Mg_{1/3}Nb_{2/3})O_3$-$0.1PbTiO_3$ single crystal (0.025 K·cm·kV^{-1})[14], $0.68Pb(Mg_{1/3}Nb_{2/3})O_3$-$0.32PbTiO_3$ thin films (0.022 K·cm·kV^{-1})[20].

As PLT20 ceramic exhibits higher *ECE* in higher temperature region, so the directly measured ΔT (40 kV/cm) are analyzed from 353.15 to 393.15 K as shown in Fig. 9a,b. It is found that a subsequent removal of electric field produces a sudden decrease in temperature (1.67 K, shown in Fig. 9b) due to electrocaloric cooling. ζ_{max} calculated from direct measurements was about 0.050 K·cm·kV^{-1}. Figure 9b shows the direct measurements under various temperatures, with increasing ambient temperatures, ΔT exhibits the maximum value at about 373.5 K. Although the temperature of maximum ΔT from theoretical calculation is higher than that of direct measurement, but they show the similar behaviours and are in good agreements. Compared to previous studies (direct measured *ECE*) on P(VDF-TrFE-CFE) film[76,77], and P(VDF-TrFE) film[78], the ΔT value in this study is smaller by one order of magnitude. But compared to that (directly measured *ECE*) of bulk materials, our measured results showed higher values than $BaHfTiO_3$ ceramics[79], $PbMg_{1/3}Nb_{2/3}O_3$–$30PbTiO_3$ single crystals[80], $PbZrO_3$ ceramics[81]. Figure 9c,d show the comparison of directly measured *ECE* reported here with some bulk materials[82–91]. For *ECE* researches on ceramics, ΔT (direct measurement) is usually very low, mostly below 1 K. Our research (maximum adiabatic temperature change) shows nearly 1.67 K, both electric field and temperatures dependent ΔT show high *ECE* values, and it may open more opportunities for practical application in refrigeration devices. The high ΔT value in this study indicates that PLT ceramics have potential applications in future solid-state refrigeration technologies.

Ferroelectrics that are characterized by the existence of an electric-field switchable polarization whose appearance is accompanied by structural phase transition have attracted increasing attention for the last 10 years especially in the field of *ECE*[74]. Some strategies to enhance the *ECE* applications are possible, such as: maximizing the number of close-energy phases near a critical point in the temperature-composition phase diagram[74], combining conventional and inverse caloric responses in a single refrigeration cycle[92,93], introducing extra available degree of freedom like strain via mechanical stress[94], and multicaloric effect driven by either single stimulus or multiple

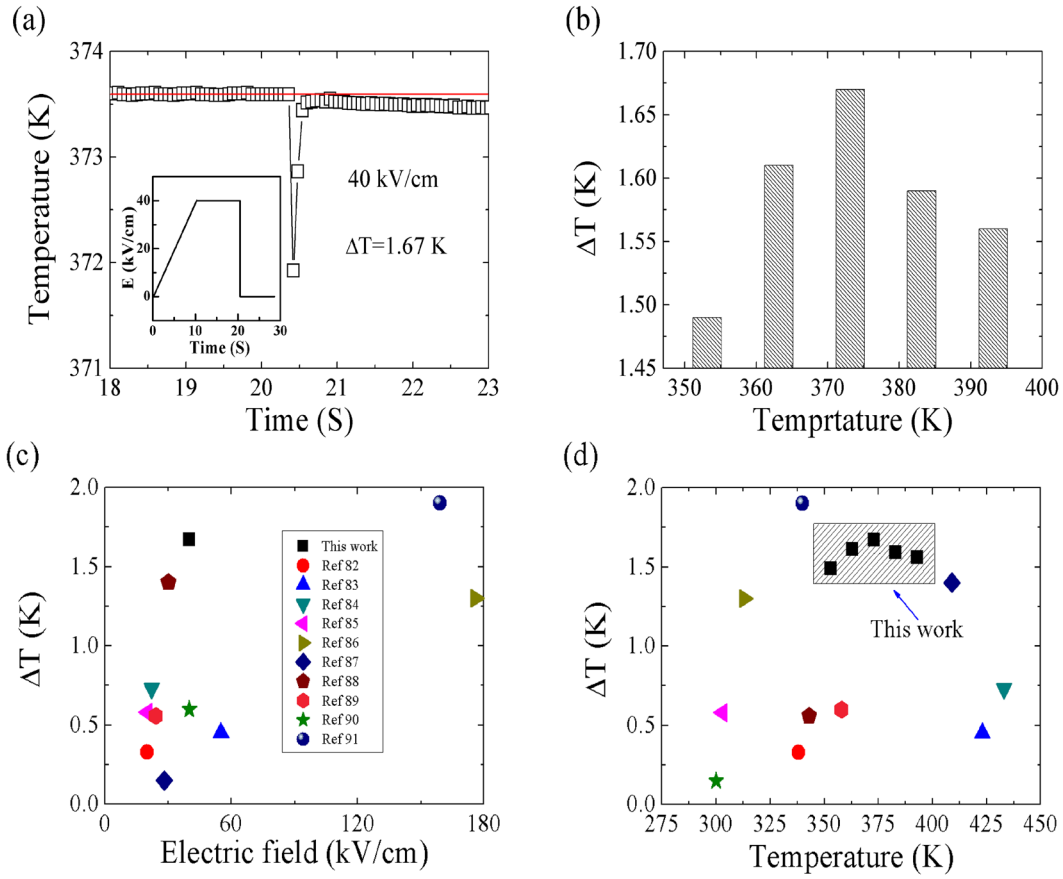

Figure 9. (**a**) Measured *ECE* data (open circles), insets show the schematic representation of the electric field pulse. (**b**) *ECE* data under various temperatures. The comparison of maximum reversible adiabatic temperature change ΔT reported under various measured electric fields (**c**) and temperatures (**d**) in this work with other bulk materials (direct measurement).

stimuli (applied/removed simultaneously or sequentially)[95]. Though promising, in bulk ferroelectrics, ΔT is usually less than a few kelvins, the obtained ΔT is still insufficient for practical application.

Conclusions

In this work, PLT ceramics are prepared and studied. Relaxer phase transitions and high temperature relaxations are studied. Room temperature energy-storage density and energy-storage efficiency are about 0.31 J/cm^3 and 91.2%, respectively. Temperatures and electric fields influenced energy-storage properties are analyzed. *ECE* is studied. High refrigeration efficiency (27.4) and large electrocaloric coefficient are achieved by theoretical calculation, maximum value of ΔT is about 1.67 K. Direct measurements of *ECE* shows that large ΔT (1.67 K) is obtained, such high value of directly measured ΔT is rare in previous reports.

References

1. Li, D. J. *et al.* Polymer piezoelectric energy harvesters for low wind speed. *Appl. Phys. Lett.* **104**, 012902 (2014).
2. Kim, D., Roh, H. S., Kim, Y., No, K. & Hong, S. Selective current collecting design for spring-type energy harvesters. *RSC Adv.* **5**, 10662 (2015).
3. Yin, S. Z. *et al.* Investigation of the electro-optic properties of electron-irradiated poly (vinylidene fluoride-trifluoroethylene) copolymer. *Opt. Eng.* **39**, 670–672 (2000).
4. Peng, B., Fan, H. & Zhang, Q. A giant electrocaloric effect in nanoscale antiferroelectric and ferroelectric phases coexisting in a relaxer $Pb_{0.8}Ba_{0.2}ZrO_3$ thin film at room temperature. *Adv. Funct. Mater.* **23**, 2987–2992 (2013).
5. Pandya, S. *et al.* Direct measurement of pyroelectric and electrocaloric effects in thin films. *Phys. Rev. Appl.* **7**, 034025 (2017).
6. Valant, M. Electrocaloric materials for future solid-state refrigeration technologies. *Prog. Mater. Sci.* **57**, 980–1009 (2012).
7. Lu, S. G. & Zhang, Q. Electrocaloric materials for solid-state refrigeration. *Adv. Mater.* **21**, 1983–1987 (2009).
8. Patel, S., Chauhan, A. & Vaish, R. Large-temperature-invariant and electrocaloric performance of modified barium titanate for solid-state refrigeration. *Energy. Tech.* **4**, 1097–1105 (2016).
9. Kriaa, I., Abdelmoula, N., Maalej, A. & Khemakhem, H. Study of the electrocaloric effect in the relaxer ferroelectric ceramic 0.75PMN-0.25PT. *J. Electron. Mater.* **44**, 4852–4856 (2015).
10. Liu, Y., Dkhil, B. & Defay, E. Spatially resolved imaging of electrocaloric effect and the resultant heat flux in multilayer capacitors. *ACS. Energy. Lett.* **1**, 521–528 (2016).
11. Luo, Z. D. *et al.* Enhanced electrocaloric effect in lead-free $BaTi_{1-x}Sn_xO_3$ ceramics near room temperature. *Appl. Phys. Lett.* **105**, 102904 (2014).
12. Bai, Y., Han, X., Ding, K. & Qiao, L. J. Combined effects of diffuse phase transition and microstructure on the electrocaloric effect in $Ba_{1-x}Sr_xTiO_3$ ceramics. *Appl. Phys. Lett.* **103**, 162902 (2013).

13. Zhou, Y. Z., Lin, Q. R., Liu, W. F. & Wang, D. Y. Compositional dependence of electrocaloric effect in lead-free (1-*x*)Ba($Zr_{0.2}Ti_{0.8}$)O_3-*x*($Ba_{0.7}Ca_{0.3}$)TiO_3 ceramics. *RSC Adv.* **6**, 14084–14089 (2016).
14. Luo, L. *et al*. Pyroelectric and electrocaloric effect of <111> -oriented 0.9PMN–0.1PT single crystal. *J. Alloys Compd.* **509**, 8149–8152 (2001).
15. Rozic, B. *et al*. Influence of the critical point on the electrocaloric response of relaxer ferroelectrics. *J. Appl. Phys.* **110**, 064118 (2011).
16. Hirose, S. *et al*. Progress on electrocaloric multilayer ceramic capacitor development. *APL Mater.* **4**, 064105 (2016).
17. Liu, B. L. *et al*. Enhanced electrocaloric effect in a $Ba_{1-x}Sr_xTiO_3$ compositionally graded film. *RSC Adv.* **4**, 24533–24537 (2014).
18. Lu, B. *et al*. Large Electrocaloric effect in relaxer ferroelectric and antiferroelectric lanthanum doped lead zirconate titanate ceramics. *Sci. Rep.* **7**, 45335 (2017).
19. Mischenko, A. S., Zhang, Q., Scott, J. F., Whatmore, R. W. & Mathur, N. D. Giant electrocaloric effect in thin-film $PbZr_{0.95}Ti_{0.05}O_3$. *Science.* **311**, 1270 (2016).
20. Feng, Z. Y., Shi, D. Q., Zeng, R. & Dou, S. X. Large electrocaloric effect of highly (100)-oriented 0.68$PbMg_{1/3}Nb_{2/3}O_3$-0.32$PbTiO_3$ thin films with a $Pb(Zr_{0.3}Ti_{0.7})O_3/PbO_x$ buffer layer. *Thin Solid Films.* **519**, 5433–5436 (2011).
21. Lu, S. G. *et al*. Organic and inorganic relaxer ferroelectrics with giant electrocaloric effect. *Appl. Phys. Lett.* **97**, 162904 (2010).
22. Kayak, G. & Alpay, S. P. Magnitude of the intrinsic electrocaloric effect in ferroelectric perovskite thin films at high electric fields. *Appl. Phys. Lett.* **90**, 252909 (2007).
23. Valant, M., Axelsson, A. K., Goupil, F. L. & Alford, N. M. Electrocaloric temperature change constrained by the dielectric strength. *Mater. Chem. Phys.* **136**, 277–280 (2012).
24. Castro, A., Ferreira, P. & Vilarinho, P. M. Block copolymer-assisted nanopatterning of porous lead titanate thin films for advanced electronics. *J. Phys. Chem. C.* **120**, 10961–10967 (2016).
25. Panigrahi, S. C., Das, P. R., Parida, B. N., Sharma, H. B. K. & Chaudhary, R. N. P. Effect of Gd-substitution on dielectric and transport properties of lead zirconate titanate ceramics. *J. Mater. Sci. Mater. Electron.* **24**, 3275–3283 (2013).
26. Shukla, A., Shukla, N. & Choudhary, R. N. P. Dielectric characteristics of La-modified $PbTiO_3$ nanoceramics. *Phase. Transit.* **90**, 362–370 (2017).
27. Kumar, P. *et al*. Influence of lanthanum substitution on dielectric properties of modified lead zirconate titanates. *Ceram. Int.* **41**, 5177–5181 (2015).
28. Yoo, H. *et al*. Visualization of three dimensional domain structures in ferroelectric $PbTiO_3$ nanotubes. *Appl. Phys. Lett.* **103**, 022902 (2013).
29. André, G., Fernando, L., Ducinei, G. & José, E. Domain structure and polarization reversal in ferroelectric lanthanum-modified lead titanate ceramics investigated by piezoresponse force microscopy. *J. Mater. Sci.* **51**, 4061–4069 (2016).
30. Kim, B., Hong, S., Ahn, G. & No, K. Synthesis of Ferroelectric Lead Titanate Nanohoneycomb Arrays via Lead Supplement Process. *J. Am. Ceram. Soc.* **99**, 2221–2225 (2016).
31. Kim, T. Y. & Jang, H. M. B-site vacancy as the origin of spontaneous normal-to-relaxor ferroelectric transitions in La-modified $PbTiO_3$. *Appl. Phys. Lett.* **77**, 3824 (2000).
32. Sayouri, S. *et al*. Diffuse phase transition and relaxor behavior in (Pb,La)TiO_3 ceramics. *Phys. Stat. Sol. (A)* **201**, 3001–3009 (2004).
33. Arnold, D. C. & Morrison, F. D. B-cation effects in relaxer and ferroelectric tetragonal tungsten bronzes. *J. Mater. Chem.* **19**, 6485–6488 (2009).
34. Hennings, D., Schnell, A. & Simon, G. Diffuse Ferroelectric Phase Transitions in $Ba(Ti_{1-y}Zr_y)O_3$ Ceramics. *J. Ceram. Soc.* **65**, 539–544 (1982).
35. Qiao, H. *et al*. Effect of Mn-doping on the structure and electric properties of 0.64$Pb(In_{0.5}Nb_{0.5})O_3$-0.36$PbTiO_3$ ceramics. *Mater. Des.* **117**, 232–238 (2017).
36. Wu, Y. R., Pu, Y. P., Zhang, P. P., Zhao, J. J. & Luo, Y. J. The relaxer behaviour and dielectric temperature stability of 0.85$BaTiO_3$-0.15$Na_{0.5}Bi_{0.5}TiO_3$-*x*$LiBa_2Nb_5O_{15}$ ceramics. *Mater. Lett.* **115**, 134–137 (2015).
37. Zhou, C. R., Liu, X. Y., Li, W. Z. & Yuan, C. L. Dielectric relaxer behaviour of A-site complex ferroelectrics of $Bi_{0.5}Na_{0.5}TiO_3$-$Bi_{0.5}K_{0.5}TiO_3$-$BiFeO_3$. *Solid. State. Commun.* **149**, 481–485 (2009).
38. Zhang, J., Yue, Z., Luo, Y., Zhang, X. & Li, L. Understanding the thermally stimulated relaxation and defect behaviour of Ti-containing microwave dielectrics: A case study of $BaTi_4O_9$. *Mater. Des.* **130**, 479–487 (2017).
39. Liu, S. F., Wu, Y. J., Li, J. & Chen, X. M. Effects of oxygen vacancies on dielectric, electrical, and ferroelectric properties of $Ba_4Nd_2Fe_2Nb_8O_{30}$ ceramics. *Appl. Phys. Lett.* **104**, 082912 (2014).
40. Zang, J. *et al*. Impedance spectroscopy of $(Bi_{1/2}Na_{1/2})TiO_3$-$BaTiO_3$ based high-temperature dielectrics. *J. Am. Ceram. Soc.* **97**, 2825–2831 (2014).
41. Wang, C., Zhang, M. & Xia, W. High-temperature dielectric relaxation in $Pb(Mg_{1/3}Nb_{2/3})O_3$-$PbTiO_3$ single crystals. *J. Am. Ceram. Soc.* **96**, 1521–1525 (2013).
42. Huang, X. X. *et al*. The dielectric anomaly and pyroelectric properties of sol-gel derived (Pb,Cd,La)TiO_3 ceramics. *J. Mater. Sci: Mater. Electron.* **26**, 3174–3178 (2015).
43. Zhang, T. F. *et al*. Oxygen-vacancy-related relaxation and conduction behavior in $(Pb_{1-x}Ba_x)(Zr_{0.95}Ti_{0.05})O_3$ ceramics. *AIP Advances.* **4**, 107141 (2014).
44. Wang, X. F. *et al*. Oxygen-vacancy-related high-temperature dielectric relaxation in $SrTiO_3$ ceramics. *J. Appl. Phys.* **107**, 114101 (2010).
45. Pelaiz-Barranco, A., Guerra, J. D. S., Noda, R. L. & Araujo, E. B. Ionized oxygen vacancy-related electrical conductivity in $(Pb_{1-x}La_x)(Zr_{0.90}Ti_{0.10})_{1-x/4}O_3$ ceramics. *J. Phys. D. Appl. Phys.* **41**, 215503 (2008).
46. Borkar, H. *et al*. Room temperature lead-free relaxer-antiferroelectric electroceramics for energy storage applications. *RSC. Adv.* 4, 22840–22847 (2014).
47. Zhang, T. F. *et al*. Energy-storage properties and high-temperature dielectric relaxation behaviours of relaxer ferroelectric $Pb(Mg_{1/3}Nb_{2/3})O_3$-$PbTiO_3$ ceramics. *J. Phys. D: Appl. Phys.* **49**, 095302 (2016).
48. Shen, Z. B., Wang, X. H., Luo, B. C. & Li, L. T. $BaTiO_3$-$BiYbO_3$ perovskite materials for energy storage applications. *J. Mater. Chem. A.* **3**, 18146–18153 (2015).
49. Yuan, C. L. *et al*. Microstructures and energy storage properties of Mn-doped 0.97$Bi_{0.47}Na_{0.47}Ba_{0.06}TiO_3-0.03K_{0.5}Na_{0.5}NbO_3$ lead-free antiferroelectric ceramics. *J. Mater. Sci: Mater. Electron.* **26**, 8793–8797 (2015).
50. Zhang, L. W., Hao, X. H., Yang, J. C., An, S. L. & Song, B. Large enhancement of energy-storage properties of compositional graded $(Pb_{1-x}La_x)(Zr_{0.65}Ti_{0.35})O_3$ relaxer ferroelectric thick films. *Appl. Phys. Lett.* **103**, 113902 (2013).
51. Hao, X. H., Zhou, J. & An, S. L. Effects of PbO content on the dielectric properties and energy storage performance of $(Pb_{0.97}La_{0.02})(Zr_{0.97}Ti_{0.03})O_3$ antiferroelectric thin films. *J. Am. Ceram. Soc.* **94**, 1647–1650 (2011).
52. Zhang, T. F. *et al*. High-temperature dielectric relaxation behaviours of relaxer-like $PbZrO_3$-$SrTiO_3$ ceramics for energy-storage applications. *Energy. Technol.* **4**, 633–640 (2016).
53. Park, M. H. *et al*. Thin $Hf_xZr_{1-x}O_2$ Films: A New Lead-Free System for Electrostatic Supercapacitors with Large Energy Storage Density and Robust Thermal Stability. *Adv. Energy. Mater.* **4**, 1400610 (2014).
54. Liu, Y. Y., Hao, X. H. & An, S. L. Significant enhancement of energy-storage performance of $(Pb_{0.91}La_{0.09})(Zr_{0.65}Ti_{0.35})O_3$ relaxer ferroelectric thin films by Mn doping. *J. Appl. Phys.* **114**, 174102 (2013).
55. Zhang, T. F. *et al*. Optical and dielectric properties of $PbZrO_3$ thin films prepared by a sol-gel process for energy-storage application. *Mater. Design.* **90**, 410–415 (2016).

56. Kim, K. D. *et al*. Scale-up and optimization of HfO_2-ZrO_2 solid solution thin films for the electrostatic supercapacitors. *Nano. Energy.* **39**, 390–399 (2017).
57. Yu, D., Xu, N. X., Hu, L., Zhang, Q. L. & Yang, H. Nanocomposites with $BaTiO_3$-$SrTiO_3$ hybrid fillers exhibiting enhanced dielectric behaviours and energy-storage densities. *J. Mater. Chem. C.* **3**, 4016–4022 (2015).
58. Wang, Y. *et al*. Optimization of energy storage density and efficiency in $Ba_xSr_{1-x}TiO_3$ ($x \leqq 0.4$) paraelectric ceramics. *Ceram. Int.* **41**, 8252–8256 (2015).
59. Zheng, J. *et al*. Dielectric characterization and energy-storage performance of lead-free niobate glass-ceramics added with La_2O_3. *Ceram. Int.* **42**, 1827–1832 (2016).
60. Li, X. Y. *et al*. Pyroelectric and electrocaloric materials. *J. Mater. Chem. C.* **1**, 23–37 (2013).
61. Lu, S. G., Tang, X. G., Wu, S. H. & Zhang, Q. M. Large electrocaloric effect in ferroelectric materials. *J. Inorg. Mater.* **29**, 6–12 (2014).
62. Mischenko, A. S., Zhang, Q., Whatmore, R. W. & Mathur, N. D. Giant electrocaloric effect in the thin film relaxer ferroelectric $0.9PbMg_{1/3}Nb_{2/3}O_3$-$0.1PbTiO_3$ near room temperature. *Appl. Phys. Lett.* **89**, 242912 (2006).
63. Goupil, F. L. *et al*. Anisotropy of the Electrocaloric Effect in Lead-Free RelaxerFerroelectrics. *Adv. Energy. Mater.* **4**, 1301688 (2014).
64. Weyland, F. *et al*. Criticality: Concept to enhance the piezoelectric and electrocaloric properties of ferroelectrics. *Adv. Funct. Mater.* **26**, 7326–7333 (2016).
65. Bai, Y., Zheng, G. P. & Shi, S. Q. Abnormal electrocaloric effect of $Na_{0.5}Bi_{0.5}TiO_3$-$BaTiO_3$ lead-free ferroelectric ceramics above room temperature. *Mater. Res. Bull.* **46**, 1866–1869 (2011).
66. Li, J. N. *et al*. Large room-temperature electrocaloric effect in lead-free $BaHf_xTi_{1-x}O_3$ ceramics under low electric field. *Acta. Mater.* **115**, 58–67 (2016).
67. Liu, X. Q., Chen, T. T., Wu, Y. J. & Chen, X. M. Enhanced Electrocaloric Effects in Spark Plasma-Sintered $Ba_{0.65}Sr_{0.35}TiO_3$-Based Ceramics at Room Temperature. *J. Am. Ceram. Soc.* **96**, 1021–1023 (2013).
68. Vrabelj, M. *et al*. Large electrocaloric effect in grain-size-engineered $0.9Pb(Mg_{1/3}Nb_{2/3})O_3$-$0.1PbTiO_3$, *J. Eur. Ceram. Soc.* **36**, 75–80 (2016).
69. Zhang, G. *et al*. Large enhancement of the electrocaloric effect in PLZT ceramics prepared by hotpressing. *APL Mater.* **4**, 064103 (2016).
70. Zhao, Y., Hao, X. H. & Zhang, Q. A giant electrocaloric effect of a $Pb_{0.97}La_{0.02}(Zr_{0.75}Sn_{0.18}Ti_{0.07})O_3$ antiferroelectric thick film at room temperature. *J. Mater. Chem. C.* **3**, 1694–1699 (2015).
71. Defay, E., Crossley, S., Kar-Narayan, S., Moya, X. & Mathur, N. D. The electrocaloric efficiency of ceramic and polymer films. *Adv. Mater.* **25**, 3337–3342 (2013).
72. Neese, B. *et al*. Large electrocaloric effect in ferroelectric polymers near room temperature. *Science.* **321**, 821–823 (2008).
73. Hao, X. H., Zhao, Y. & Zhang, Q. Phase structure tuned electrocaloric effect and pyroelectric energy harvesting performance of $(Pb_{0.97}La_{0.02})(Zr,Sn,Ti)O_3$ antiferroelectric thick films. *J. Phys. Chem. C.* **119**, 18877–18885 (2015).
74. Qian, X. S. *et al*. Giant electrocaloric response over a broad temperature range in modified $BaTiO_3$ ceramics. *Adv. Funct. Mater.* **24**, 1300–1305 (2014).
75. Jiang, X. J. *et al*. Electrocaloric effect based on the depolarization transition in $(1-x)Bi_{0.5}Na_{0.5}TiO_3$-$xKNbO_3$ lead-free ceramics. *Ceram. Int.* **40**, 2627–2634 (2014).
76. Lu, S. G. *et al*. Comparison of directly and indirectly measured electrocaloric effect in relaxor ferroelectric polymers. *Appl. Phys. Lett.* **97**, 202901 (2010).
77. Ma, R. *et al*. Highly efficient electrocaloric cooling with electrostatic actuation. *Science.* **357**, 1130–1134 (2017).
78. Lu, S. G. *et al*. Enhanced electrocaloric effect in ferroelectric poly(vinylidene-fluoride /trifluoroethylene) 55/45 mol % copolymer at ferroelectric-paraelectric transition. *Appl. Phys. Lett.* **98**, 122906 (2011).
79. Crossley, S. *et al*. Direct electrocaloric measurement of $0.9Pb(Mg_{1/3}Nb_{2/3})O_3$-$0.1PbTiO_3$ films using scanning thermal microscopy. *Appl. Phys. Lett.* **108**, 032902 (2016).
80. Goupil, F. L. *et al*. Direct and indirect electrocaloric measurements on <001> -$PbMg_{1/3}Nb_{2/3}O_3$-$30PbTiO_3$ single crystals. *J. Appl. Phys.* **111**, 124109 (2012).
81. Pirc, R., Rožič, B., Koruza, J., Malič, B. & Kutnjak, Z. Negative electrocaloric effect in antiferroelectric $PbZrO_3$. *EPL.* **107**, 17002 (2014).
82. Sanlialp, M., Shvartsman, V. V., Acosta, M., Dkhil, B. & Lupascu, D. C. Strong electrocaloric effect in lead-free $0.65Ba(Zr_{0.2}Ti_{0.8})O_3$-$0.35(Ba_{0.7}Ca_{0.3})TiO_3$ ceramics obtained by direct measurements. *Appl. Phys. Lett.* **106**, 062901 (2015).
83. Axelsson, A. K., Goupil, F. L., Valant, M. & Alford, N. M. Electrocaloric effect in lead-free Aurivillius relaxer ferroelectric ceramics. *Acta. Mater.* **124**, 120–126 (2017).
84. Goupil, F. L. *et al*. Electrocaloric enhancement near the morphotropic phase boundary in lead-free NBT-KBT ceramics. *Appl. Phys. Lett.* **107**, 172903 (2015).
85. Molin, C. *et al*. Effect of dopants on the electrocaloric effect of $0.92Pb(Mg_{1/3}Nb_{2/3})O_3$-$0.08PbTiO_3$ ceramics. *J. Eur. Ceram. Soc.* **35**, 2065–2071 (2015).
86. Bai, Y., Zheng, G. & Shi, S. Direct measurement of giant electrocaloric effect in $BaTiO_3$ multilayer thick film structure beyond theoretical prediction. *Appl. Phys. Lett.* **96**, 192902 (2010).
87. Wang, J., Yang, T., Wei, K. & Yao, X. Temperature-electric field hysteresis loop of electrocaloric effect in ferroelectricity-Direct measurement and analysis of electrocaloric effect. *Appl. Phys. Lett.* **102**, 152907 (2013).
88. Novak, N., Pirc, R. & Kutnjak, Z. Impact of critical point on piezoelectric and electrocaloric response in barium titanate. *Phys. Rev. B.* **87**, 104102 (2013).
89. Hagberg, J., Uusimäki, A. & Jantunen, H. Electrocaloric characteristics in reactive sintered $0.87Pb(Mg_{1/3}Nb_{2/3})O_3$-$0.13PbTiO_3$. *Appl. Phys. Lett.* **92**, 132909 (2008).
90. Wang, J. *et al*. Nonadiabatic direct measurement electrocaloric effect in lead-free $Ba,Ca(Zr,Ti)O_3$ ceramics. *J. Alloys. Compd.* **550**, 561–563 (2013).
91. Koruza, J. *et al*. Large electrocaloric effect in lead-free $K_{0.5}Na_{0.5}NbO_3$-$SrTiO_3$ ceramics. *Appl. Phys. Lett.* **106**, 202905 (2015).
92. Geng, W. P. *et al*. Giant Negative Electrocaloric Effect in Antiferroelectric La-Doped $Pb(ZrTi)O_3$ Thin Films Near Room Temperature. *Adv. Mater.* **27**, 3165 (2015).
93. Liu, Y. *et al*. Giant Room-Temperature Elastocaloric Effect in Ferroelectric Ultrathin Films. *Adv. Mater.* **26**, 6132 (2014).
94. Liu, Y. *et al*. Prediction of giant elastocaloric strength and stress-mediated electrocaloric effect in $BaTiO_3$ single crystals. *Phys. Rev. B.* **90**, 104107 (2014).
95. Moya, X., Kar-Narayan, S. & Mathur, N. D. Caloric materials near ferroic phase transitions. *Nat. Mater.* **13**, 439 (2014).

Acknowledgements

This work was supported by the National Natural Science Foundation of China (Grant No. 11574057), the Guangdong Provincial Natural Science Foundation of China (Grant No. 2016A030313718), and the Science and Technology Program of Guangdong Province of China (Grant Nos. 2016A010104018, and 2017A010104022).

Author Contributions

T.F.Z. analyzed the data and wrote the paper, X.X.H. contributed to dielectric and impedance measurement. X.G.T. supervised the project and participated in the paper correction. Y.P.J. and Q.X.L. contributed to the dielectric and ferroelectric analysis. B.L. and S.G.L. contributed to the electrocaloric measurements. All authors read and approved the final manuscript.

Additional Information

Competing Interests: The authors declare that they have no competing interests.

Publisher's note: Springer Nature remains neutral with regard to jurisdictional claims in published maps and institutional affiliations.